RSC Applied Interfaces

ROYAL SOCIETY OF CHEMISTRY

PAPER

View Article Online
View Journal

Cite this: DOI: 10.1039/d6lf00041j

Highly oxidation-resistant imidazolium-modified catechol for stable wet adhesion under alkaline conditions

Kan Wang,†[a] Yue Xu,†[b] Fatemeh Razaviamri,[a] Chunling Zhang,[c] Zhihui Zhang,[b] Bo Liu*[b] and Bruce P. Lee*[a]

Premature oxidation of catechol drastically reduces its adhesion strength and utility. This study chemically linked catechol to an imidazolium group, which functioned as an intrinsic protecting group that retarded catechol oxidation and enabled stable wet adhesion under basic conditions. Johnson–Kendall–Roberts (JKR) contact mechanical testing was performed to determine the work of adhesion (W_{adh}) of imidazolium-modified catechol (VIMCAT), which remained unchanged for up to 48 hours when incubated at pH 7.4. Contrastingly, W_{adh} values of unprotected catechol were quickly reduced by over 25% within 30 minutes. VIMCAT still retained its initial adhesion strength even after incubation at pH 9 for over 2 hours. Electron spin resonance (ESR) and ultraviolet-visible (UV-vis) spectra confirmed that VIMCAT resisted conversion to quinone under alkaline conditions. VIMCAT is intrinsically more resistant to oxidation as demonstrated by a higher anodic potential observed from the cyclic voltammetry (CV) experiment and a lower highest occupied molecular orbital (HOMO) energy level calculated using density functional theory (DFT) analysis when compared to unmodified catechol. The direct conjugation of imidazolium with catechol offers a metal-free and intrinsically stabilizing molecular design for a high-performance adhesive polymer, capable of long-term operation in alkaline environments.

Received 14th February 2026,
Accepted 26th April 2026

DOI: 10.1039/d6lf00041j

rsc.li/RSCApplInter

Introduction

The outstanding underwater adhesion of mussels has inspired the development of functional adhesive materials over the past decades.[1,2] Mussels secrete adhesive proteins that are rich in the catecholic amino acid, 3,4-dihydroxy-L-phenylalanine (DOPA), which enables these mussel foot proteins (mfps) to bind to wide ranges of wet surfaces.[3,4] Catechol engages in multiple interfacial and intermolecular interactions such as hydrogen bonding, metal coordination, π–π stacking and π–cation interactions, which impart catechol-conjugated polymers with strong adhesive properties.[5] Many researchers have created catechol-functionalized adhesives and coatings for many applications, ranging from cell encapsulation and delivery, adhesive hydrogels for localized immunomodulation, to non-cytotoxic wound closure tapes.[6–8] However, the adhesive property of catechol drastically decreases upon autoxidation in neutral to basic pH conditions.[9,10] This decrease in adhesion and premature oxidation greatly limit the utility of catechol-containing adhesives. While the formation of transient complexes with boronic acid and metal ions such as Fe^{3+} or Al^{3+} can temporarily stabilize catechol against oxidation,[11–14] these approaches only provide temporary protection and adhesion strength of the protected catechol is diminished.[15] Therefore, more effective strategies are needed to prevent catechol oxidation while maintaining its adhesive functionality.

Natural mfps found at the adhesive-surface interface (*e.g.*, mfp-3 and mfp-5) remained highly adhesive despite the alkaline nature of seawaters (pH 7.5 to 8.5).[16,17] These proteins contain a large abundance of lysine residues, which enables cation–π complexation between the positively charged lysine and the electron-rich catechol groups.[18] The cation pulls electron density away from the aromatic ring,[19,20] making the catechol moiety more resistant to oxidation. Synthetic analogues that combined catechol with a cationic functional group have demonstrated reduced rate of catechol oxidation.[21–24] Similarly, chemical modification of catechol with an electron-withdrawing group (EWG) has also increased the oxidation resistance of catechol.[25–28] The EWG pulls electrons from the phenol moiety through resonance and inductive effects, which increases the oxidation potential of

[a] Biomedical Engineering Department, Michigan Technologi-cal University, 1400 Townsend Drive, Houghton, Michigan, 49931, USA. E-mail: bplee@mtu.edu
[b] Key Laboratory of Bionic Engineering, Ministry of Educa-tion, Jilin University, Changchun, Jilin, China. E-mail: lbb1107@jlu.edu.cn
[c] School of Materials Science and Engineering, Jilin University, Changchun 130022, China
† KW and YX contributed equally to this work.

catechol.[29] However, these studies have only demonstrated short-term stability in preserving the adhesive property of catechol (*e.g.*, up to 30 minutes at pH 7) and catechol quickly oxidized at elevated pH levels.[21,30] Thus, a longer-lasting and stable adhesive analogue with improved oxidation resistance will be needed to improve the utility and flexibility in utilizing catechol as the adhesive moiety.

In this work, we explored the effect of imidazolium-catechol conjugation on the oxidation resistance and adhesion preservation of catechol under basic conditions (Scheme 1). Direct coupling of the electron-poor imidazolium to catechol provides an electron-withdrawing effect on the catechol group.[31,32] Additionally, the positively charged imidazolium group can form cation–π interaction with catechol and provide an additional electron-withdrawing effect on the catechol group.[33,34] π–π interactions between the imidazolium ring and aromatic ring of catechol can also provide added protection. The cationic ring acts as a π acceptor to form π^{+}–π electron donor–acceptor interactions with the electron-rich aromatic ring of catechol functioning as the π donor.[35,36] Imidazolium-based ionic liquids have also been reported to promote polyphenol extraction potentially through enhancing the stability of the polyphenols.[37–39]

Inspired by these findings, we functionalized catechol with an imidazolium group to mitigate catechol oxidation and to preserve its adhesive property under alkaline pH conditions. We synthesized a polymerizable monomer consisting of a vinyl imidazolium group and a catechol moiety abbreviated as VIMCAT (Scheme 1b) and copolymerized it with 2-methoxyethyl acrylate (MEA) to form an adhesive polymer, P(MEA-*co*-VIMCAT). Catechol containing monomer, dopamine methacrylamide (DMA), and polymer (P(MEA-*co*-DMA)) were utilized as the controls. The effect of prolonged incubation (0.5 to 72 hours) in a solution with an alkaline pH (pH 7.4, 8, 8.5 and 9) on the adhesive property of P(MEA-*co*-VIMCAT) was evaluated through Johnson–Kendall–Roberts (JKR) contact mechanics testing using four different surface substrates: borosilicate glass (SiO_2), amine-functionalized glass (NH_2), titanium (Ti), and polystyrene (PS). Complementary characterization techniques, including electron spin resonance (ESR) and ultraviolet-visible (UV-vis) spectroscopy were employed to elucidate the oxidation state of imidazolium-modified catechol. Cyclic voltammetry (CV) and density functional theory (DFT) simulations were employed to evaluate the redox potential of catechol as a result of imidazolium conjugation.

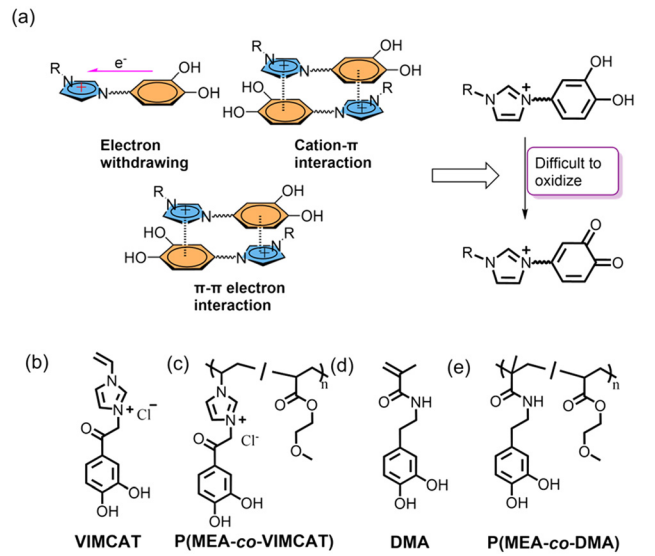

Scheme 1 (a) The imidazolium cation engages in multiple stabilizing interactions with the catechol group, including electron-withdrawing effect through direct conjugation as well as cation–π and π–π interactions. These interactions enhance the oxidation resistance of catechol. Chemical structures of (b) VIMCAT, (c) P(MEA-*co*-VIMCAT), (d) DMA and (e) P(MEA-*co*-DMA).

Results and discussion

Synthesis and characterization of VIMCAT and adhesive polymers

VIMCAT was synthesized through a one-step Menshutkin reaction to obtain a polymerizable monomer bearing vinyl, imidazolium chloride, and catechol moieties (Fig. S1). The reaction proceeded with an excellent yield exceeding 90%. Proton nuclear magnetic resonance (^{1}H NMR) spectroscopy confirmed the expected chemical structure of VIMCAT, including the imidazolium ring (9.53, 8.32 and 7.87 ppm), benzene ring (7.50, 7.48, and 7.46 ppm), phenolic hydroxyl group (10.41 and 9.68 ppm), and vinyl protons (6.02, 5.99 and 5.47 ppm) (Fig. S2). The FT-IR spectrum of VIMCAT (Fig. S3) displays a peak at 1161 cm^{-1} corresponding to C–N stretching of the imidazolium ring, confirming successful quaternization. A broad absorption between 3243–3515 cm^{-1} is attributed to O–H stretching vibrations from the catechol group. Linear adhesive copolymers were subsequently synthesized *via* thermally initiated free-radical polymerization using MEA as the backbone monomer and either VIMCAT or DMA as the adhesive comonomer. The copolymer compositions, determined from ^{1}H NMR integration, revealed consistent molar ratios of MEA to adhesive monomer (10 : 1) in both adhesive polymers (Fig. S4 and S5). The resulting polymers were designated as P(MEA-*co*-VIMCAT) and P(MEA-*co*-DMA), respectively.

GPC analysis showed that P(MEA-*co*-VIMCAT) possessed a substantially higher $\bar{M}_n$ (274.2 kDa) compared to P(MEA-*co*-DMA) (7.3 kDa) (Table S1 and Fig. S6). The polydispersity index ($Đ$) values were 4.7 and 3.0 for P(MEA-*co*-VIMCAT) and P(MEA-*co*-DMA), respectively. The markedly lower molecular weight of P(MEA-*co*-DMA) is attributed to the partial inhibition of radical polymerization by the unprotected catechol groups.[40] The catechol sidechain possesses a strong radical-scavenging ability, reducing effective chain propagation and resulting in shorter P(MEA-*co*-DMA) chains. In contrast, the radical-scavenging ability of the VIMCAT is

attenuated by the presence of the imidazolium moiety, leading to a weaker inhibitory effect on free-radical chain growth. Additionally, imidazole-based monomers are highly reactive and often results in polymers with elevated molecular weights.[41,42] As a result, chain propagation is more favorable, ultimately yielding P(MEA-*co*-VIMCAT) with a significantly higher molecular weight than P(MEA-*co*-DMA). However, the elevated reactivity of imidazole-based monomers often results in uneven chain growth and large $Đ$ values using conventional free radical polymerization approach.[41,42]

Nevertheless, the adhesive monomer content in both copolymers was identical based on ^{1}H NMR (Fig. S4 and S5), suggesting that molecular weight differences would not significantly affect the interfacial bonding energy measured using JKR contact mechanics testing.[43] Unlike bulk adhesion tests (*e.g.*, lap shear test) where the mechanical property and the performance of the adhesive is highly dependent on the molecular weight of a polymer,[44] JKR contact mechanics test probes the interfacial binding interactions between the adhesive coating and the contacting surface with minimal contribution from the bulk cohesive properties.[45]

Adhesion testing using JKR contact mechanics test setup

JKR contact mechanics test was utilized to determine the work of adhesion (W_{adh}) between a borosilicate glass surface and the adhesive coating wetted by a buffer solution (Fig. 1, S7 and S8). To investigate the effect of solution pH on the adhesive property of catechol, adhesive coatings were incubated for 0.5 to 72 hours in solutions buffered at pH 7.4, 8, 8.5 and 9.0 prior to adhesion contact. For P(MEA-*co*-VIMCAT), W_{adh} values averaged around 1.0 J m^{-2} after 30 minutes of incubation regardless of the pH of the buffer. When incubating at pH 7.4, W_{adh} values did not change for over 48 hours and the value did not decrease until the 72-hour time point. When the pH of the buffer was increased, W_{adh} values started to decrease at an earlier time point. However, P(MEA-*co*-VIMCAT) still demonstrated remarkable resistance to autoxidation and was able to maintain its initial W_{adh} values for 24, 4, and 2 hours when incubated at pH 8, 8.5, and 9, respectively. Adhesion results for P(MEA-*co*-VIMCAT) demonstrated the exceptional stability of catechol when tethered to an imidazolium group.

In contrast, P(MEA-*co*-DMA) exhibited rapid loss of adhesion under basic conditions. For comparison purposes, W_{adh} values were compared with P(MEA-*co*-DMA) incubated at pH 3 (W_{adh} = 0.95 ± 0.06 J m^{-2}) to provide the adhesive property of the unoxidized form of catechol.[46] This W_{adh} value is comparable with that of initial value for P(MEA-*co*-VIMCAT) (1.0 J m^{-2}), which confirmed that molecular weight of the polymers had minimal impact in the measured values. The W_{adh} values of P(MEA-*co*-DMA) decreased progressively with increasing pH, showing a decrease of 23%, 61%, 78%, and 79% after exposure to pH 7.4, 8.0, 8.5, and 9.0, respectively, for merely 30 minutes. This rapid decrease in adhesion is consistent with the well-established autoxidation of catechol at neutral to basic pH.[37] Within only 2 to 4 hours of incubation, W_{adh} values have decreased by more than 90%

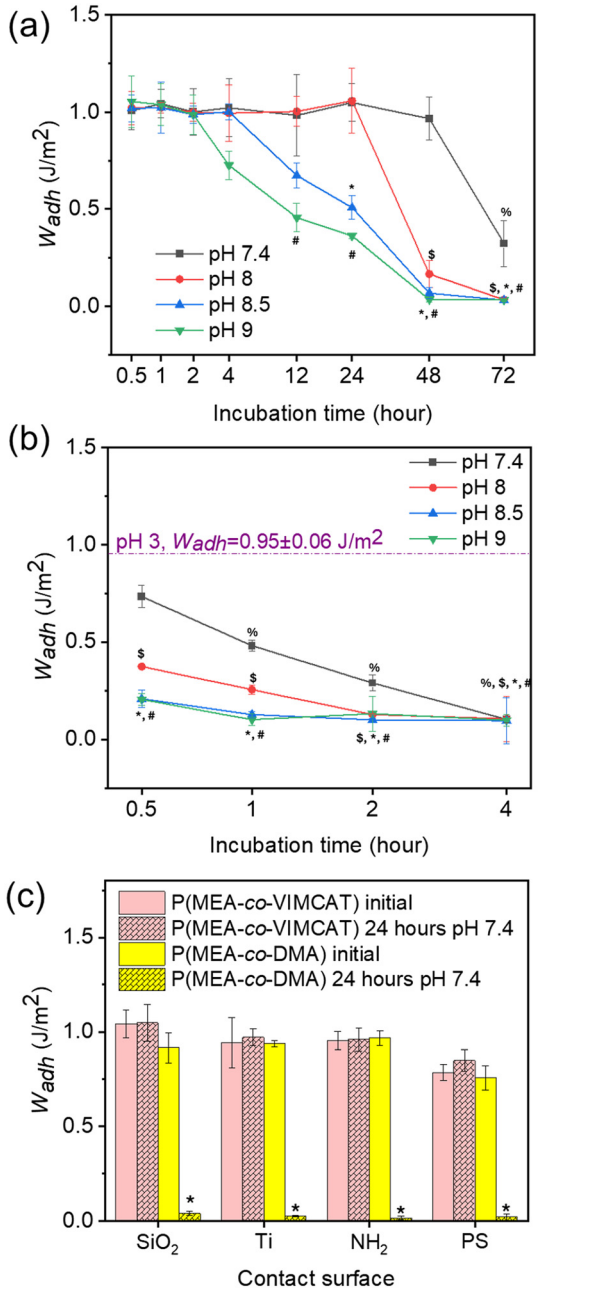

Fig. 1 W_{adh} of (a) P(MEA-*co*-VIMCAT) and (b) P(MEA-*co*-DMA) contacting borosilicate glass after the adhesive coatings were incubated for different amounts of time at different pH levels. Dashed line in (b) corresponds to P(MEA-*co*-DMA) tested after 1 hour incubation in pH 3. $^{\%,\$,*,\#}P < 0.05$ when compared to the initial W_{adh} measured at pH 7.4, 8, 8.5, and 9, respectively. (c) W_{adh} of P(MEA-*co*-VIMCAT) and P(MEA-*co*-DMA) when contacting different surfaces before and after incubation at pH 7.4 buffer for 24 hours. For P(MEA-co-VIMCAT), the initial value was obtained after 1 hour of incubation at pH 7.4. For P(MEA-co-DMA), the initial value was obtained after 1 hour of incubation at pH 3. $^{*}P < 0.05$ when compared to the initial adhesion.

and remained at this low level thereafter, indicating near-complete deactivation.

To examine the interfacial bonding behavior of P(MEA-*co*-VIMCAT) with various types of surfaces, four different surface substrates (SiO_2, Ti, NH_2, and PS) were brought into contact with the adhesive coating (Fig. 1c, S9 and S10). Initially, both polymers exhibit strong adhesion to all four surfaces through interfacial hydrogen bonds (SiO_2 and NH_2), metal coordination bonds (Ti), and π–π interaction (PS).[46,47] After 24 hours of incubation at pH 7.4, P(MEA-*co*-VIMCAT) retained its initial W_{adh} values across all the substrates tested, demonstrating excellent chemical stability and wet adhesion. On the other hand, P(MEA-*co*-DMA) exhibited complete loss of adhesion to all substrates after 24 hours of incubation at pH 7.4. Although *in situ* oxidization of catechol promote Schiff-base and Michael addition reactions with primary amine groups, the amine-coated surface was brought into contact with P(MEA-*co*-DMA) after it had been incubated in pH 7.4 solution for 24 h and had ceased to be reactive. While the adhesion between catechol and PS occurs primarily through π–π interaction, P(MEA-*co*-DMA) demonstrated weak adhesion to PS after 24 hours of incubation. This observation suggests the autoxidation of catechol to quinone with a conjugated cyclic dione structure that cannot effectively engage in π–π interaction with PS.[48] This result further confirms that the loss of adhesion originates from the oxidation of catechol moieties in P(MEA-*co*-DMA).

The adhesion results underscore the stabilizing effect of imidazolium in preserving catechol's adhesive properties. While the imidazolium protection is temporary, it significantly retarded the rate of catechol oxidation when compared to the unmodified catechol and prolonged adhesive functionality under basic conditions. Cationic functional groups have previously been reported to promote interfacial bonding to negative charged surfaces.[24,25,48] The pK_a values for silica vary from 4.5 to 8.5 depending on the arrangement of the SiOH surface,[49–51] and the SiO_2 surface will carry negative charges at the pH ranges tested in our experiments. However, the initial W_{adh} values for P(MEA-*co*-VIMCAT) and P(MEA-*co*-DMA) are comparable and W_{adh} values decreased over time, which indicates that catechol moieties contributed the most towards interfacial bonding behavior in our system.

Chemical analysis on the oxidation state of catechol

The oxidative stability of catechol was assessed using ESR with 5,5-dimethylpyrroline *N*-oxide (DMPO) as a spin-trapping agent (Fig. 2). For VIMCAT, no detectable signals corresponding to semiquinone or quinone species were observed for the first 4 hours of incubation at pH 9, indicating a pronounced delay in the onset of oxidation. The combined signal for semiquinone and quinone was not observed until after 6 hours of incubation.[52,53] For DMA, distinct ESR signals corresponding to semiquinone radicals appeared immediately after incubation in a pH 9 buffer.[54]

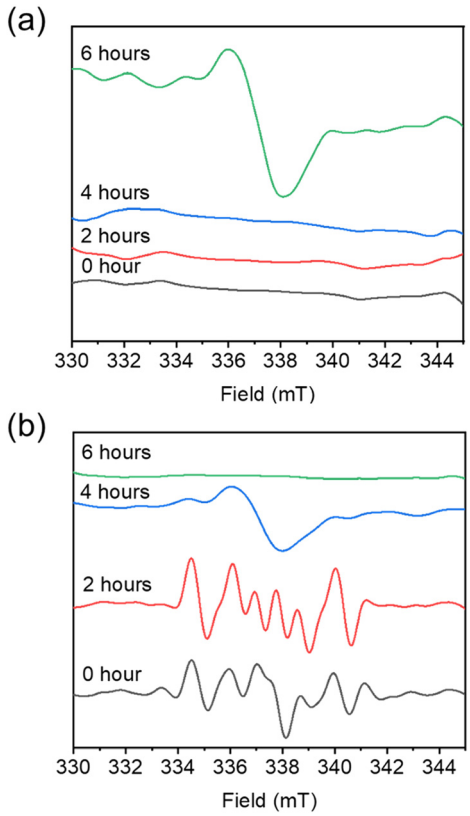

Fig. 2 ESR spectra of (a) VIMCAT and (b) DMA incubated at pH 9 measured at different time points.

The signal intensity increased over time with the appearance of quinone peaks at the 4-hour time point that is consistent with the oxidation pathways of catechol. The observed temporal shift demonstrates the oxidation-inhibiting effect of the imidazolium group and preserving the adhesive properties of catechol.

From UV-vis spectra of both P(MEA-*co*-VIMCAT) and P(MEA-*co*-DMA) exhibited a characteristic catechol absorption peak at 280 nm (Fig. 3).[55] P(MEA-*co*-VIMCAT) exhibits an additional peak at 316 nm can be attributed to the π → π* transition of the catechol group in VIMCAT and the n → π* transition originating from the lone pair electrons of C═O.[56] Under alkaline conditions, the merging and shifting of these peaks can be explained by solvation effects arising from the interaction between dimethyl sulfoxide (DMSO) and the buffer system. However, even with increasing pH, P(MEA-*co*-VIMCAT) displayed no discernible oxidation-related absorption in the 400–600 nm range, which typically corresponds to the formation of quinone species.[57] In contrast, P(MEA-*co*-DMA) exhibited a new absorption peak at around 510 nm characteristic of catechol oxidation, which is accompanied by a decrease in intensity for the catechol characteristic peak (280 nm) indicating a conversion of catechol to *o*-quinone.[57]

To elucidate the molecular mechanism underlying the long-term adhesive stability of VIMCAT, we extended our investigation to analyze its antioxidant capacity from the

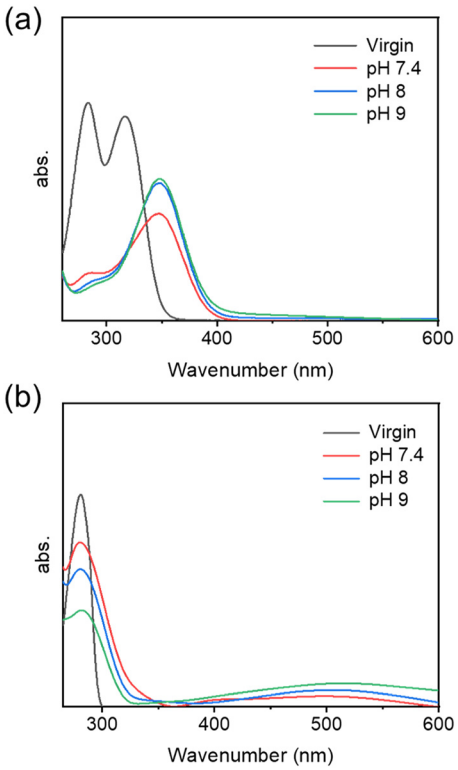

Fig. 3 UV-vis spectra of (a) P(MEA-*co*-VIMCAT) and (b) P(MEA-*co*-DMA) after 2 hours of incubation with different alkaline pH buffers.

perspectives of electronic structure and electrochemical properties. The highest occupied molecular orbital (HOMO) energy level serves as a key indicator for evaluating the electron-donating ability of a molecule.[58] A lower HOMO energy level indicates greater resistance to oxidation due to a higher ionization potential.[59] DFT calculations were performed to compare the HOMO energy levels of the VIMCAT and DMA monomers (Fig. 4). The calculated HOMO energy of VIMCAT (−5.45 eV) was lower than that of DMA (−4.77 eV), suggesting that VIMCAT is intrinsically more resistant to oxidation.

From CV experiments, VIMCAT exhibited two anodic peaks (A1, A2) and two cathodic peaks (B1, B2) (Fig. 4c, Table S2). The first anodic peak (A1) corresponds to the loss of one electron from the catechol group to form a semiquinone radical, followed by a second oxidation step at A2 leading to complete conversion into *o*-quinone. During the reduction, the semiquinone intermediate regains one electron at B1, accompanied by Li^+ ion insertion, and acquires a second electron at B2 to regenerate the catechol structure. These observation compared favorably with previously reported imidazolium-conjugated catechol.[31,32] In contrast, DMA displayed three pairs of anodic and cathodic peaks (Fig. 4d). Peaks C1 and C2 correspond to the stepwise oxidation of catechol groups, whereas C3 is attributed to oxidation of the imine moiety in the DMA unit.[60] The corresponding reduction processes are represented by peaks D1, D2, and D3 (Table S3). Importantly, the second anodic peak (A2) of VIMCAT appeared at +0.76 V, substantially higher than the corresponding oxidation peak of DMA at +0.48 V. This anodic shift signifies that VIMCAT requires a higher potential to oxidize, consistent with its lower HOMO energy level and enhanced oxidative stability.[61] Together, the computational and electrochemical analyses confirm that incorporation of the imidazolium moiety effectively stabilizes the catechol group by lowering its HOMO energy level, thereby impeding oxidation. These findings align closely with the JKR adhesion results, reinforcing that VIMCAT maintains superior oxidation resistance and adhesion durability under alkaline conditions.

Taken together, we developed a molecular strategy to overcome the intrinsic oxidation instability of catechol-based

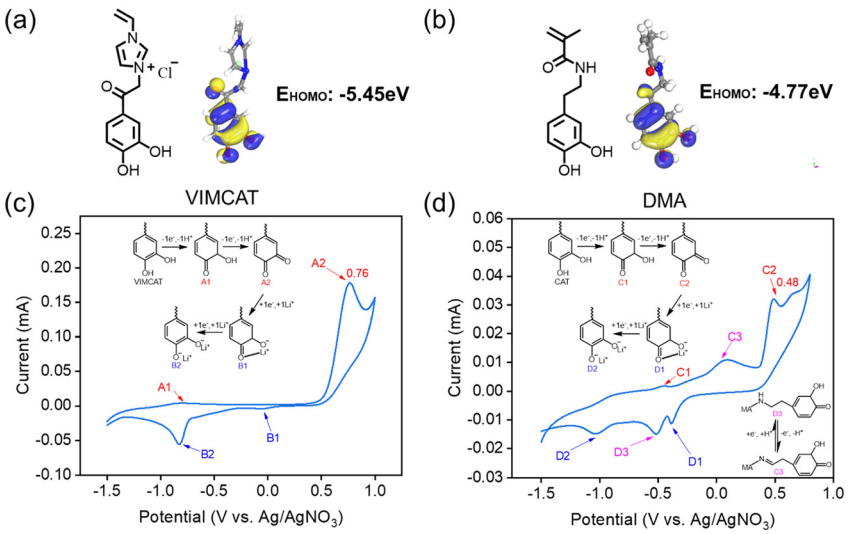

Fig. 4 Calculated HOMO energy level of (a) VIMCAT and (b) DMA. CV curves of (c) VIMCAT and (d) DMA recorded at a scan rate of 50 mV s^{-1} for solutions containing 5 mM of the monomer and 0.5 M of LiTFSI in anhydrous DMSO.

adhesives by designing an imidazolium modified catechol monomer, VIMCAT. Through adhesion testing and combined spectroscopic, electrochemical, and computational analyses, we demonstrated that the incorporation of imidazolium cation greatly stabilized catechol under oxidative conditions. Most notably, VIMCAT demonstrated unprecedented adhesion stability after incubation at pH 7.4 for over 48 hours. The adhesive property of VIMCAT did not change even after incubation for over 2 hours at pH 9. These observations significantly increased the utility and flexibility when using catechol as an adhesive molecule, while minimizing risks associated with premature catechol oxidation. Our DFT experiment examined the electronic structure of a single molecule of VIMCAT, which can be attributed to the electron withdrawing effect associated with the direct conjugation between catechol and imidazolium. However, our modeling experiment did not investigate the added electron withdrawing effects associated with intermolecular π–π, cation–π and H-bonding interactions,[35,36] which will be a subject of future investigations. Nevertheless, our reported data collectively demonstrated the contribution of imidazolium-conjugation on retarding the rate of catechol oxidation and preservation of catechol adhesion in an alkaline environment.

Various chemical modification strategies have been reported to improve the oxidation resistance of catechol.[25–28] Particularly, a catechol analogue, hydroxypyridinone (HOPO), was reported by Degen *et al.*[21] to demonstrate pH-tolerant wet adhesion at a neutral pH. Additionally, incorporation of an anionic carboxylic acid into a polymer network has been utilized to buffer pH within the adhesive matrix and retarded catechol oxidation.[46] However, these strategies have only preserved catechol adhesion for up to 30 min at pH 7, and catechol quickly oxidized at a higher pH. Although reversible complexes formed between boronic acid with catechol limits its oxidation, the adhesive property of catechol also decreased.[15,62,63] Recently, salicylhydroxamic acid (SHAM) was reported as a new catechol analogue that demonstrated equivalent of better adhesive properties when compared that of catechol and chemical stability against irreversible oxidation.[64,65] However, SHAM's adhesive properties diminish with increasing pH.[48] In contrast to these prior reports, VIMCAT demonstrated a significant improvement in increasing the stability of catechol while preserving its adhesive properties at basic pH.

Although adhesive monomer prepared *via* direct conjugation between catechol and an imidazolium salt was previously reported, a 4-step synthesis was required to prepare the catechol-vinyl imidazolium monomer in these prior reports.[31,32] Additionally, oxidation resistant nature of the adhesive was not investigated in these prior studies. In contrast, the polymerizable VIMCAT monomer reported here was synthesized using a simple 1-step synthesis with a high yield (>90%), which makes it a more viable synthetic route in creating large batches of adhesive polymers. This molecular design deepens our understanding of redox-controlled adhesion mechanisms and provides a scalable framework for developing next generation mussel-inspired adhesives that are resilient under chemically and mechanically demanding environments.

Conclusions

The imidazolium modified catechol adhesive demonstrated exceptional oxidation resistance and stable wet adhesion under basic conditions. Adhesion of VIMCAT remained stable in pH 7.4 for as long as 48 hours, while the unmodified catechol rapidly lost its adhesion strength through autoxidation within 30 minutes. ESR and UV-vis spectra verified that imidazolium functionalization retarded the rate of catechol oxidation. DFT and CV analyses revealed a lower HOMO energy level and higher oxidation potential for VIMCAT, respectively, rendering the adhesive molecule more resistant to autoxidation. Our data correlated the stable adhesion of VIMCAT with its enhanced oxidation resistance at basic pH. This self-protecting molecular design offers a robust platform for long-lasting adhesives that maintain strong, reliable performance in alkaline environments.

Experiments

Materials

2-Chloro-3′,4′-dihydroxyacetophenone (CCDP), 1-vinylimidazole (VIM), MEA, ethanol, hydrochloric acid (HCl), sodium hydroxide (NaOH), silver nitrate ($AgNO_3$), DMSO (HPLC grade), dimethylformamide (DMF), poly(vinylidene fluoride) (PVDF) in 1-methyl-2-pyrrolidinone (NMP), diethyl ether, phosphate-buffered saline (PBS), acetonitrile, silicon oil, dimethyl sulfoxide-d_6 (DMSO-d_6), DMPO, (3-aminopropyl) trimethoxysilane (APTS), and LiTFSI were purchased from Sigma-Aldrich (St. Louis, MO). 2,2′-Azobis(isobutyronitrile) (AIBN) was purchased from Wako Pure Chemical Industries, Ltd. (Osaka, Japan). SiO_2 hemispheres (1/4″ diameter) were purchased from ISP Optics (Orlando, FL). NH_2 was prepared by treating SiO_2 with APTS following a published protocol.[62] Ti (1/4″ diameter) and PS (1/4″ diameter) balls were purchased from McMaster-carr (Elmhurst, IL). The buffers, including pH 7.4, pH 8, pH 8.5 and pH 9, were prepared using deionized (DI) water, PBS, and NaOH. DMA was synthesized following a previously published protocol.[66]

Preparation of VIMCAT

VIMCAT was synthesized *via* a Menshutkin reaction between CCDP and VIM (Fig. S1). CCDP (373 mg, 2.0 mmol, 1.0 equiv) and VIM (207 mg, 2.2 mmol, 1.1 equiv) were dissolved in 10 mL of absolute ethanol (200 proof). The reaction mixture was stirred at 500 rpm under a nitrogen atmosphere at 80 °C for 16 h. The resulting precipitate was collected by vacuum filtration, washed with ethanol (3 × 5 mL), and dried under vacuum overnight to afford VIMCAT as a pale gray solid (530 mg, 95% isolated yield).

Preparation of adhesive polymers

Adhesive polymers were synthesized by free-radical polymerization (Fig. S1). 10.0 mmol MEA (1.3 mL), 1.0 mmol VIMCAT (266 mg), and 0.3 mmol AIBN (49 mg) were dissolved in 10 mL DMF. The solution was stirred at 500 rpm and heated in a 70 °C silicone oil bath under nitrogen atmosphere 12 hours. The synthesized linear polymer was precipitated in diethyl ether. The product was subsequently dialyzed against deionized water acidified to pH = 3 using concentrated HCl for 48 hours to remove unreacted monomers and lyophilized to yield P(MEA-*co*-VIMCAT) (40% isolated yield). A catechol-containing polymer was prepared following the same procedure using DMA instead of VIMCAT to prepare P(MEA-*co*-DMA) (60% isolated yield).

Characterization of adhesive monomers and polymers

For ^{1}H NMR characterization, 20 mg of monomer or polymer was dissolved in 0.5 mL of DMSO-d_6 and analyzed using a 500 MHz spectrometer (Ascend, Bruker, MA). The relative integration values of characteristic peaks were used to determine the molar composition of functional groups within the adhesive polymers. Molecular weight characterization was performed using GPC (Shimadzu HPLC Nexera Series, Kyoto, JP) equipped with a Shodex OHpak LB-803 column, a UV detector (SPD-40, Shimadzu), a refractive index detector (RID-20A, Shimadzu), and a multi-angle light scattering detector (miniDAWN, Wyatt). Polymers were dissolved in HPLC-grade DMSO at a concentration of 5 mg mL^{-1} and filtered with a polypropylene filter (25 mm diameter; 0.2 μm pore size; VWR). Elution was carried out using HPLC-grade DMF as the mobile phase at a flow rate of 0.5 mL per minutes and a column temperature of 40 °C. The weight average molecular weight ($\bar{M}_w$), number-average molecular weight ($\bar{M}_n$), and polydispersity index ($Đ$) of the synthesized linear polymers were evaluated.

To assess catechol oxidation under basic conditions, 0.05 mmol of VIMCAT or DMA and 0.10 mmol DMPO were dissolved in 1 mL of pH 9 PBS buffer. At predetermined time intervals (0–6 hours), solution samples were withdrawn using glass capillaries and immediately analyzed by ESR spectroscopy (Magnettech ESR5000, Bruker, Billerica, MA, USA). UV-vis spectroscopy was performed using solutions from mixing 20 μL of polymer solution (20 mM of polymer in DMSO) with 1980 μL of PBS buffered at pH 7.4, 8.0, or 9.0 by UV-vis spectrophotometer (MAPADA, China). CV analysis was performed using an electrochemical workstation (CHI660F, Chenhua, China) in an anhydrous DMSO solution containing 5 mM VIMCAT or DMA and 0.5 M LiTFSI as the supporting electrolyte. A standard three-electrode configuration was employed, comprising a glassy carbon working electrode (area = 0.07 cm^2), a platinum wire counter electrode, and a silver reference electrode (0.01 M $AgNO_3$ in acetonitrile). Voltammetric curves were recorded at scan rates of 50 mV s^{-1} at room temperature.

JKR contact mechanics test

A custom-built JKR contact mechanics device was used to study adhesive properties. The JKR setup consists of an indenter (ALS-06, Transducer Techniques), a 10 g load cell (Transducer Techniques), and a high-resolution miniature linear stage stepper motor (MFA-PPD, Newport).[15,63] One of four types of hemispheric surfaces was affixed to the indenter and utilized as the contacting surface. The hemispheres included SiO_2, Ti, NH_2, or PS.

Adhesive precursor solutions were prepared by dissolving the adhesive polymer and PVDF in NMP at a weight ratio of 9 : 1 and further diluted to a final polymer concentration of 150 mg mL^{-1}. PVDF was utilized as the non-adhesive binder to form a cohesive film.[65] 20 μL of the precursor solution was drop-cast onto pre-cleaned glass slides and allowed to dry overnight in a fume hood to ensure complete solvent evaporation. The resulting adhesive coatings were rinsed several times with DI water to remove residual NMP and then air-dried prior to testing. The adhesive coatings were incubated in buffer solutions with pH values ranging from 7.4 to 9 for 0.5–72 hours prior to adhesion testing.

Prior to each test, the coating surface was wetted with 15 μL of buffer solution (same pH as the incubation buffer). The hemisphere was brought into contact with the adhesive coating at a speed of 1 μm s^{-1} until a preload of 10 mN was reached. The surface contact was maintained at the same force for 60 seconds and the indenter was retracted at the same speed. Based on a rigid spherical surface onto a thin coating JKR model, the work of adhesion (W_{adh}) is equal to the critical energy release rate (G_c), calculated by the maximum adhesion force (F_{max}) and the radius (R) of the hemisphere:[43,67,68]

$$W_{adh} = G_c = \frac{2}{3\pi R} F_{max} \quad (1)$$

DFT simulation

HOMO energy levels of VIMCAT and DMA were calculated using the DMol^3 module in Materials Studio based on DFT within the generalized gradient approximation (GGA). The Perdew–Burke–Ernzerhof (PBE) functional was employed for all calculations. Structural optimization was performed with the following convergence criteria: energy change $<1.0 \times 10^{-5}$ Ha, maximum force <0.002 Ha Å^{-1}, and maximum displacement <0.005 Å. Following geometry optimization, the orbital energies were computed at the GGA-PBE level to determine the HOMO values.

Statistical analysis

Statistical analysis was performed *via* R Project software. One-way analysis of variance (one-way ANOVA) with Tukey method was used for comparing multiple groups, using a p-value of 0.05.

Author contributions

KW: conceptualization, methodology, data curation, investigation, validation, formal analysis, writing – review &

editing, writing – original draft. YX: methodology, software, data curation, investigation, validation, formal analysis, visualization, writing – original draft, writing – review & editing. FR: data curation, writing – original draft. CZ: resources, writing – original draft. ZZ: resources, writing – original draft. BL: formal analysis, supervision, writing – original draft, writing – review & editing. BPL: writing – original draft, writing – review & editing, project administration, funding acquisition, supervision, formal analysis.

Conflicts of interest

The authors declare no competing financial interest.

Data availability

Data will be made available upon request.

Supplementary information: the supporting information (SI) is available free of charge. Schematic diagram of the drop casting method, NMR and FTIR spectra, GPC characterization, CV redox peaks, contact curves.

Acknowledgements

This project was funded by the National Science Foundation under award number CMMI 2119019, the National Institutes of Health under award number R15GM135875, and the Office of Naval Research under award number N00014-21-1-2877.

References

1 Z. Zhou, X. Ning, W. Wei, H. Lu, H. Wen, H. Zeng, Y. Chen, J. Liu, Y. Xie and P. Hu, Dual-Network Hydrogel Loaded With ROS-activated Hydrogen Sulfide Donor to Accelerate Wound Healing and Inhibit Scar Production, *Adv. healthc. mater.*, 2025, e2500264.
2 Q. Guo, J. Chen, J. Wang, H. Zeng and J. Yu, Recent progress in synthesis and application of mussel-inspired adhesives, *Nanoscale*, 2020, **12**, 1307–1324.
3 B. K. Ahn, Perspectives on Mussel-Inspired Wet Adhesion, *J. Am. Chem. Soc.*, 2017, **139**, 10166–10171.
4 J. H. Waite, Mussel adhesion - essential footwork, *J. Exp. Biol.*, 2017, **220**, 517–530.
5 W. Dou, X. Zeng, S. Zhu, Y. Zhu, H. Liu and S. Li, Mussel-Inspired Injectable Adhesive Hydrogels for Biomedical Applications, *Int. J. Mol. Sci.*, 2024, **25**, 9100.
6 W. Zhang, R. Wang, Z. Sun, X. Zhu, Q. Zhao, T. Zhang, A. Cholewinski, F. K. Yang, B. Zhao and R. Pinnaratip, Catechol-functionalized hydrogels: biomimetic design, adhesion mechanism, and biomedical applications, *Chem. Soc. Rev.*, 2020, **49**, 433–464.
7 C. Xie, Y. Li, X. Guo, Y. Ding, X. Lu and S. Rao, Mussel-inspired adhesive hydrogels for local immunomodulation, *Mater. Chem. Front.*, 2023, **7**, 846–872.
8 P. Ni, Y. Chen, K. Wan, Y. Cheng, Y. Fang, Y. Weng and H. Liu, Mussel Foot Protein-Inspired Adhesive Tapes with Tunable Underwater Adhesion, *ACS Appl. Mater. Interfaces*, 2024, **16**, 45550–45562.
9 H. Lee, N. F. Scherer and P. B. Messersmith, Single Molecule Mechanics of Mussel Adhesion, *Proc. Natl. Acad. Sci. U. S. A.*, 2006, **103**, 12999–13003.
10 S. Xu, M. Kang, X. Xin, J. Liang, H. Xiao, Y. Lu, J. Yang and H. Zhai, Design principles and application research of mussel-inspired materials: A review, *J. Environ. Chem. Eng.*, 2024, **12**, 111655.
11 L. Terriac, J.-J. Helesbeux, Y. Maugars, J. Guicheux, M. W. Tibbitt and V. Delplace, Boronate ester hydrogels for biomedical applications: challenges and opportunities, *Chem. Mater.*, 2024, **36**, 6674–6695.
12 B. Liu, J. Li, Z. Zhang, J. D. Roland and B. P. Lee, pH responsive antibacterial hydrogel utilizing catechol–boronate complexation chemistry, *Chem. Eng. J.*, 2022, **441**, 135808.
13 L. Malacaria, G. A. Corrente, A. Beneduci, E. Furia, T. Marino and G. Mazzone, A Review on Coordination Properties of Al(III) and Fe(III) toward Natural Antioxidant Molecules: Experimental and Theoretical Insights, *Molecules*, 2021, **26**, 2603.
14 Z. Xu, Mechanics of metal-catecholate complexes: The roles of coordination state and metal types, *Sci. Rep.*, 2013, **3**, 2914.
15 A. R. Narkar, B. Barker, M. Clisch, J. Jiang and B. P. Lee, pH Responsive and Oxidation Resistant Wet Adhesive based on Reversible Catechol-Boronate Complexation, *Chem. Mater.*, 2016, **28**, 5432–5439.
16 Q. Lu, E. Danner, J. H. Waite, J. N. Israelachvili, H. Zeng and D. S. Hwang, Adhesion of mussel foot proteins to different substrate surfaces, *J. R. Soc. Interface*, 2013, **10**, 20120759.
17 J. Yu, W. Wei, M. S. Menyo, A. Masic, J. H. Waite and J. N. Israelachvili, Adhesion of Mussel Foot Protein-3 to TiO2 Surfaces: the Effect of pH, *Biomacromolecules*, 2013, **14**, 1072–1077.
18 M. A. Gebbie, W. Wei, A. M. Schrader, T. R. Cristiani, H. A. Dobbs, M. Idso, B. F. Chmelka, J. H. Waite and J. N. Israelachvili, Tuning underwater adhesion with cation–π interactions, *Nat. Chem.*, 2017, **9**, 473–479.
19 D. A. Dougherty, Cation-π Interactions Involving Aromatic Amino Acids1234, *J. Nutr.*, 2007, **137**, 1504S–1508S.
20 D. A. Dougherty, The Cation–π Interaction in Chemistry and Biology, *Chem. Rev.*, 2025, **125**, 2793–2808.
21 G. D. Degen, S. T. Ahmed, P. R. Stow, A. Butler and R. C. Andresen Eguiluz, pH-Tolerant Wet Adhesion of Catechol Analogs, *ACS Appl. Mater. Interfaces*, 2024, **16**, 22689–22695.
22 M. Shin, Y. Park, S. Jin, Y. M. Jung and H. J. Cha, Two faces of amine–catechol pair synergy in underwater cation– π interactions, *Chem. Mater.*, 2021, **33**, 3196–3206.
23 G. Degen and J. Israelachvili, Unravelling the Secrets of Catechol-Cation Binding Synergy, *Biophys. J.*, 2018, **114**, 542a.
24 G. P. Maier, M. V. Rapp, J. H. Waite, J. N. Israelachvili and A. Butler, Adaptive synergy between catechol and lysine promotes wet adhesion by surface salt displacement, *Science*, 2015, **349**, 628–632.

25 G. P. Maier, C. M. Bernt and A. Butler, Catechol oxidation: considerations in the design of wet adhesive materials, *Biomater. Sci.*, 2018, **6**, 332–339.
26 M. S. Menyo, C. J. Hawker and J. H. Waite, Versatile tuning of supramolecular hydrogels through metal complexation of oxidation-resistant catechol-inspired ligands, *Soft Matter*, 2013, **9**, 10314–10323.
27 E. Amstad, A. U. Gehring, H. Fischer, V. V. Nagaiyanallur, G. Hähner, M. Textor and E. Reimhult, Influence of electronegative substituents on the binding affinity of catechol-derived anchors to Fe3O4 nanoparticles, *J. Phys. Chem. C*, 2011, **115**, 683–691.
28 B. Liu, C. Zhou, Z. Zhang, J. D. Roland and B. P. Lee, Antimicrobial property of halogenated catechols, *Chem. Eng. J.*, 2021, **403**, 126340.
29 H.-Y. Zhang, Y.-M. Sun and D.-Z. Chen, O–H Bond Dissociation Energies of Phenolic Compounds are Determined by Field/Inductive Effect or Resonance Effect?A DFT Study and Its Implication, *Quant. Struct.-Act. Relat.*, 2001, **20**, 148–152.
30 R. Borraccino, M. Kharoune, R. Giot, S. N. Agathos, E.-J. Nyns, H. P. Naveau and A. Pauss, Abiotic transformation of catechol and 1-naphthol in aqueous solution—Influence of environmental factors, *Water Res.*, 2001, **35**, 3729–3737.
31 N. Patil, D. Cordella, A. Aqil, A. Debuigne, S. Admassie, C. Jérôme and C. Detrembleur, Surface- and Redox-Active Multifunctional Polyphenol-Derived Poly(ionic liquid)s: Controlled Synthesis and Characterization, *Macromolecules*, 2016, **49**, 7676–7691.
32 N. Patil, M. Aqil, A. Aqil, F. Ouhib, R. Marcilla, A. Minoia, R. Lazzaroni, C. Jérôme and C. Detrembleur, Integration of Redox-Active Catechol Pendants into Poly(ionic liquid) for the Design of High-Performance Lithium-Ion Battery Cathodes, *Chem. Mater.*, 2018, **30**, 5831–5835.
33 X. Feng, W. Gao, S. Zhou, H. Shi, H. Huang and W. Song, Discrimination and simultaneous determination of hydroquinone and catechol by tunable polymerization of imidazolium-based ionic liquid on multi-walled carbon nanotube surfaces J, *Anal. Chim. Acta*, 2013, **805**, 36–44.
34 H. Wei, X.-S. Wu, G.-Y. Wen and Y. Qiao, Imidazolium Ionic Liquid Functionalized Carbon Nanotubes for Improved Interfacial Charge Transfer and Simultaneous Determination of Dihydroxybenzene Isomers J, *Molecules*, 2016, **21**, 617.
35 F. Xiao and J. J. Pignatello, π+–π Interactions between (Hetero)aromatic Amine Cations and the Graphitic Surfaces of Pyrogenic Carbonaceous Materials, *Environ. Sci. Technol.*, 2015, **49**, 906–914.
36 N. J. Singh, S. K. Min, D. Y. Kim and K. S. Kim, Comprehensive Energy Analysis for Various Types of π-Interaction, *J. Chem. Theory Comput.*, 2009, **5**, 515–529.
37 T. V. Dinh, P. S. Saravana, H. C. Woo and B. S. Chun, Ionic liquid-assisted subcritical water enhances the extraction of phenolics from brown seaweed and its antioxidant activity J, *Sep. Purif. Technol.*, 2018, **196**, 287–299.
38 Y. Lu, W. Ma, R. Hu, X. Dai and Y. Pan, Ionic liquid-based microwave-assisted extraction of phenolic alkaloids from the medicinal plant Nelumbo nucifera Gaertn, *J. Chromatogr. A*, 2008, **1208**, 42–46.
39 S. T. M. Vidal, M. J. N. Correia, M. M. Marques, M. R. Ismael and M. T. A. Reis, Studies on the Use of Ionic Liquids as Potential Extractants of Phenolic Compounds and Metal Ions J, *Sep. Sci. Technol.*, 2005, **39**, 2155–2169.
40 B. P. Lee, K. Huang, F. N. Nunalee, K. R. Shull and P. B. Messersmith, Synthesis of 3,4-dihydroxyphenylalanine (DOPA) containing monomers and their co-polymerization with PEG-diacrylate to form hydrogels, *J. Biomater. Sci., Polym. Ed.*, 2004, **15**, 449–464.
41 M. H. Allen, Jr., S. T. Hemp, A. E. Smith and T. E. Long, Controlled Radical Polymerization of 4-Vinylimidazole, *Macromolecules*, 2012, **45**, 3669–3676.
42 H. Mori, M. Yahagi and T. Endo, RAFT Polymerization of N-Vinylimidazolium Salts and Synthesis of Thermoresponsive Ionic Liquid Block Copolymers, *Macromolecules*, 2009, **42**, 8082–8092.
43 K. R. Shull, Contact mechanics and the adhesion of soft solids, *Mater. Sci. Eng.: R: Rep.*, 2002, **36**, 1–45.
44 C. L. Jenkins, H. J. Meredith and J. J. Wilker, Molecular Weight Effects upon the Adhesive Bonding of a Mussel Mimetic Polymer, *ACS Appl. Mater. Interfaces*, 2013, **5**, 5091–5096.
45 M. Ciavarella, J. Joe, A. Papangelo and J. R. Barber, The role of adhesion in contact mechanics, *J. R. Soc. Interface*, 2019, **16**, 20180738.
46 A. R. Narkar, J. D. Kelley, R. Pinnaratip and B. P. Lee, Effect of Ionic Functional Groups on the Oxidation State and Interfacial Binding Property of Catechol-Based Adhesive, *Biomacromolecules*, 2018, **19**, 1416–1424.
47 Z. Tachan, I. Hod and A. Zaban, The TiO2–Catechol Complex: Coupling Type II Sensitization with Efficient Catalysis of Water Oxidation, *Adv. Energy Mater.*, 2014, **4**, 1301249.
48 K. Wang, L. Patra, B. Liu, Z. Zhang, R. Pandey and B. P. Lee, Salicylhydroxamic Acid as a Novel Switchable Adhesive Molecule, *Chem. Mater.*, 2023, **35**, 5322–5330.
49 C. Hu, L. Yu, Z. Zheng, J. Wang, Y. Liu, Y. Jiang, G. Tong, Y. Zhou and X. Wang, Tannin as a gatekeeper of pH-responsive mesoporous silica nanoparticles for drug delivery, *RSC Adv.*, 2015, **5**, 85436–85441.
50 S. Ong, X. Zhao and K. B. Eisenthal, Polarization of water molecules at a charged interface: second harmonic studies of the silica/water interface, *Chem. Phys. Lett.*, 1992, **191**, 327–335.
51 E. Tombácz and M. Szekeres, Colloidal behavior of aqueous montmorillonite suspensions: the specific role of pH in the presence of indifferent electrolytes, *Appl. Clay Sci.*, 2004, **27**, 75–94.
52 S. Saab and L. Neto, Characterization by Electron Paramagnetic Resonance of organic matter in whole soil (Gleysoil) and organic-mineral fractions, *J. Braz. Chem. Soc.*, 2008, **19**, 413–417.
53 J. Mitra and S. Sarkar, Modelling the reduced xanthine oxidase in active sulfo and inactive desulfo forms, *Dalton*

Trans., 2013, **42**, 3050–3058.

54 M. Mochizuki, S.-i. Yamazaki, K. Kano and T. Ikeda, Kinetic analysis and mechanistic aspects of autoxidation of catechin, *Biochim. Biophys. Acta*, 2002, **1569**, 35–44.

55 H. Meng, P. K. Forooshani, P. U. Joshi, J. Osborne, X. Mi, C. Meingast, R. Pinnaratip, J. Kelley, A. Narkar, W. He, M. C. Frost, C. L. Heldt and B. P. Lee, Biomimetic recyclable microgels for on-demand generation of hydrogen peroxide and antipathogenic application, *Acta Biomater.*, 2019, **83**, 109–118.

56 N. Syafni, D. P. Putra and D. Arbain, 3,4-Dihydroxybenzoic acid and 3,4-Dihydroxybenzaldehyde from the fern trichomanes chinense L.; isolation, antimicrobial and antioxidant properties, *Indones. J. Chem.*, 2012, **12**, 273–278.

57 A. Abebe, D. Zheng, J. Evans and M. Sugumaran, Reexamination of the mechanisms of oxidative transformation of the insect cuticular sclerotizing precursor, 1,2-dehydro-N-acetyldopamine, *Insect Biochem. Mol. Biol.*, 2010, **40**, 650–659.

58 L.-C. Wang, H.-K. Chen, W.-J. Wang, F.-Y. Hsu, H.-Z. Huang, R.-T. Kuo, W.-P. Li, H.-K. Tian and C.-S. Yeh, Boosting Upconversion Efficiency in Optically Inert Shelled Structures with Electroactive Membrane through Electron Donation J, *Adv. Mater.*, 2024, **36**, e2404120.

59 S. Li, L. Ye, W. Zhao, H. Yan, B. Yang, D. Liu, W. Li, H. Ade and J. Hou, A Wide Band Gap Polymer with a Deep Highest Occupied Molecular Orbital Level Enables 14.2% Efficiency in Polymer Solar Cells, *J. Am. Chem. Soc.*, 2018, **140**, 7159–7167.

60 M. Mehrdadian, S. Khazalpour and A. Amani, Electrochemical synthesis of new quinone-imines with assisted of 4-ethynylaniline and para-toluidine as nucleophile, *Electrochim. Acta*, 2022, **427**, 140849.

61 N. Elgrishi, K. Rountree, B. McCarthy, E. Rountree, T. Eisenhart and J. Dempsey, A Practical Beginner's Guide to Cyclic Voltammetry, *J. Chem. Educ.*, 2018, **95**, 197–206.

62 A. R. Narkar, C. Kendrick, K. Bellur, T. Leftwich, Z. Zhang and B. P. Lee, Rapidly responsive smart adhesive-coated micropillars utilizing catechol-boronate complexation chemistry, *Soft Matter*, 2019, **15**, 5474–5482.

63 M. S. A. Bhuiyan, B. Liu, J. Manuel, B. Zhao and B. P. Lee, Effect of Conductivity on In Situ Deactivation of Catechol–Boronate Complexation-Based Reversible Smart Adhesive, *Biomacromolecules*, 2021, **22**, 4004–4015.

64 K. Wang, V. Khare, A. A. Das, F. Razaviamri and B. P. Lee, Salicylhydroxamic acid as an electro-responsive and switchable adhesive molecule, *Chem. Sci.*, 2026, DOI: 10.1039/D5SC07881D.

65 M. S. A. Bhuiyan, K. Wang, F. Razaviamri and B. P. Lee, Salicylhydroxamic acid containing structural adhesive, *RSC Appl. Polym.*, 2024, **2**, 838–846.

66 M. S. A. Bhuiyan, J. D. Roland, B. Liu, M. Reaume, Z. Zhang, J. D. Kelley and B. P. Lee, In Situ Deactivation of Catechol-Containing Adhesive Using Electrochemistry, *J. Am. Chem. Soc.*, 2020, **142**, 4631–4638.

67 M. Ciavarella, J. Joe, A. Papangelo and J. Barber, The role of adhesion in contact mechanics, *J. R. Soc. Interface*, 2019, **16**, 20180738.

68 S. T. Choi, Extended JKR theory on adhesive contact of a spherical tip onto a film on a substrate, *J. Mater. Res.*, 2012, **27**, 113–120.